

Hairygami: Analysis of DNA Nanostructure’s Conformational Change Driven by Functionalizable Overhangs

Matthew Sample,^{1,2} Michael Matthies,² and Petr Šulc²

¹*School for Engineering of Matter, Transport, and Energy,
Arizona State University, Tempe, AZ 85287, USA*

²*School of Molecular Sciences and Center for Molecular Design and Biomimetics,
The Biodesign Institute, Arizona State University,
1001 South McAllister Avenue, Tempe, Arizona 85281, USA*

DNA origami is a widely used method to construct nanostructures by self-assembling designed DNA strands. These structures are often used as "breadboards" for templated assembly of proteins, gold nanoparticles, aptamers, and other molecules, with applications ranging from therapeutics and diagnostics to plasmonics and photonics. Imaging these structures using AFM or TEM is not capable to capture their full conformation ensemble as they only show their structure flattened on a surface. However, certain conformations of the nanostructure can position guest molecules into distances unaccounted for in their intended design, thus leading to spurious interactions between guest molecules that are designed to be separated. Here, we use molecular dynamics simulations to capture conformational ensemble of 2D DNA origami tiles and show that introducing single-stranded overhangs, which are typically used for functionalization of the origami with guest molecules, induces a curvature of the tile structure in the bulk. We show that the shape deformation is of entropic origin, with implications for design of robust DNA origami breadboards as well as potential approach to modulate structure shape by introducing overhangs.

I. INTRODUCTION

The emerging fields of DNA and RNA nanotechnology use DNA or RNA strands to self-assemble nanoscale structures and devices. The fields have multiple promising applications that include therapeutics, diagnostics, molecular computing, biotemplated assembly for nanophotonics and optical computing, nano-electronics, and synthetic biology [1–5].

Currently, the most popular construct in DNA nanotechnology is the DNA origami [6]. It typically consists of a single-stranded DNA scaffold strand taken from M13 bacteriophage (7249 bases long), and short staple strands that are complementary to different regions of the scaffold strand that then self-assemble a structure of a desired shape. Originally, DNA origami were designed as 2D structures, and later work has extended this concept to 3D [7]. The origami designs have been very quickly adopted by the broad bionanotechnology research community because DNA strands can be functionalized e.g. by attaching gold nanoparticles, proteins, small molecules, quantum dots and aptamers [8–11]. Given the fact that we know where each nucleotide is going to be positioned with respect to the rest of the structure in the final assembled shape, the DNA origami technique effectively provides nanoscale precision for positioning objects with respect to each other. A common strategy to introduce these functional moieties to DNA origamis is to extend the strands comprising the structure with single-stranded overhangs (Fig. 2). However, it has not been previously explored how such modifications can affect the structure of the origami, and therefore potentially its function as well.

Typically, DNA origami structures are characterized by surface-based techniques like atomic force microscopy

(AFM) and transmission electron microscopy (TEM). During this analysis the structure is adhered to a charged surface, limiting the number of conformations that can be observed. While this is not playing a role for applications in molecular electronics, molecular medicine and diagnostics assays often rely on the interactions of the structures in solution, and hence the images produced by AFM and TEM imaging techniques are not necessarily representative of the conformations that the structures sample in solution. 3D nanostructures have also been characterized by cryo-EM techniques [12, 13]. However, the image processing and reconstruction of 3D DNA nanostructures in high resolution remains a challenging process, which relies on automated construction of an ensemble average, and hence it can still miss some conformations. Flexible DNA structures sample in the bulk highly deformed conformations [14], potentially impacting their function such as when different functionalized regions that are not supposed to interact with each other might appear in close proximity, or when the attached particles are not at the distances intended in the design.

Currently, there is no experimental technique available that would allow for easy, reliable and high-precision characterization of the conformational ensemble of DNA origami nanostructures. Super-resolution imaging-based approaches, such as DNA-PAINT [15], or small angle X-ray scattering (SAXS) can provide information about conformations in the bulk [16], but ideally need to be accompanied by a model that can inform the measurements for improvement of signal to noise ratio in analysis. Here, we show how computational modeling can provide crucial insight into the flexibility and motion of 2D DNA origami structures, and in particular focus on conformational ensemble changes induced by DNA overhangs attached to the nanostructure. Modeling of DNA

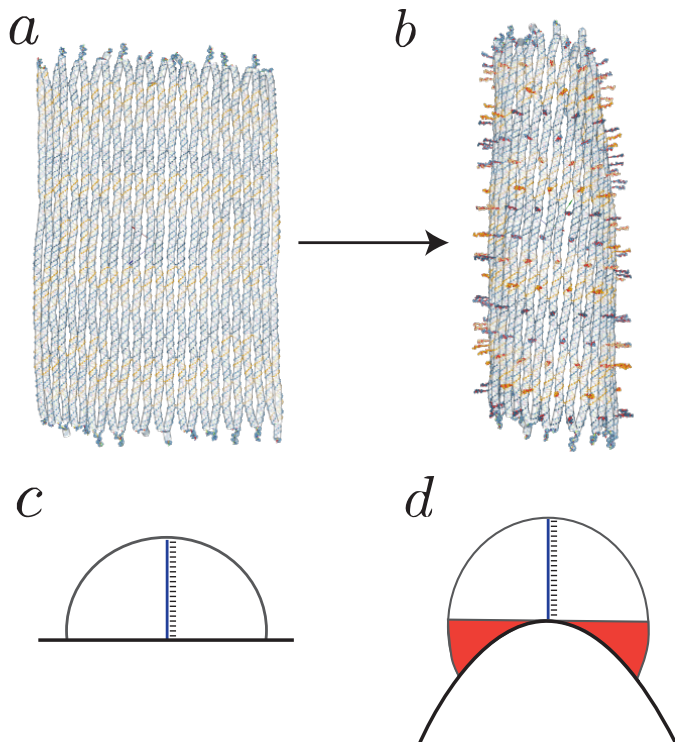


FIG. 1. The addition of overhangs causes a 2D DNA origami tile (*a*) to adopt a curved shape (*b*). The origin of the curvature is mainly due to the entropic preference of the overhang sequences: on the curved surface (shown schematically as a side view of an overhang in (*d*)) they have more accessible conformational space than they do on the flat surface (*c*).

origami can present significant challenges, however, given the sizes of the DNA origamis of over 14 000 nucleotides. Atomistic resolution modeling is limited to at most microseconds timescales, and hence over the past several years coarse-grained models [17–20] and finite-element based predictions approaches have been developed to computationally sample DNA origami mean shape [21–24]. In this study, we use the nucleotide-level coarse-grained model oxDNA [17, 18, 25, 26], as it has been shown to accurately capture both single-stranded and double-stranded DNA biophysics [27, 28]. It is parameterized to reproduce thermodynamic, mechanical and structural properties of both single-stranded and double-stranded DNA [17]. The model has been used to study a range of DNA nanotechnology systems, and where available, good agreement with experimental results has been found [27].

We use the oxDNA model to study the effects of 2D DNA origami deformation induced by the presence of single-stranded and double-stranded overhangs. An enhanced sampling method was utilized to sample the conformational space of the structure. We show that bent conformations are significantly enhanced as longer or denser overhangs are attached to the origami (Fig. 1). We show that the effect is of entropic origin, with the highly bent conformation being more favorable for struc-

tures with longer and denser overhangs. The results have implications both for DNA origami designs used for cargo delivery or surface-bound strand displacement based computation [29, 30], as the attached overhangs can have unintended effects on the structures’ conformational ensemble. At the same time, the mechanism of entropy-induced curvature of DNA origami tiles can be exploited to impose certain preferred shapes to DNA structures. We study here the effects of overhang length and density at different temperatures and salt concentrations, and show how the distribution of different shapes of the DNA tile is affected by their presence.

II. RESULTS

A. Studied Systems

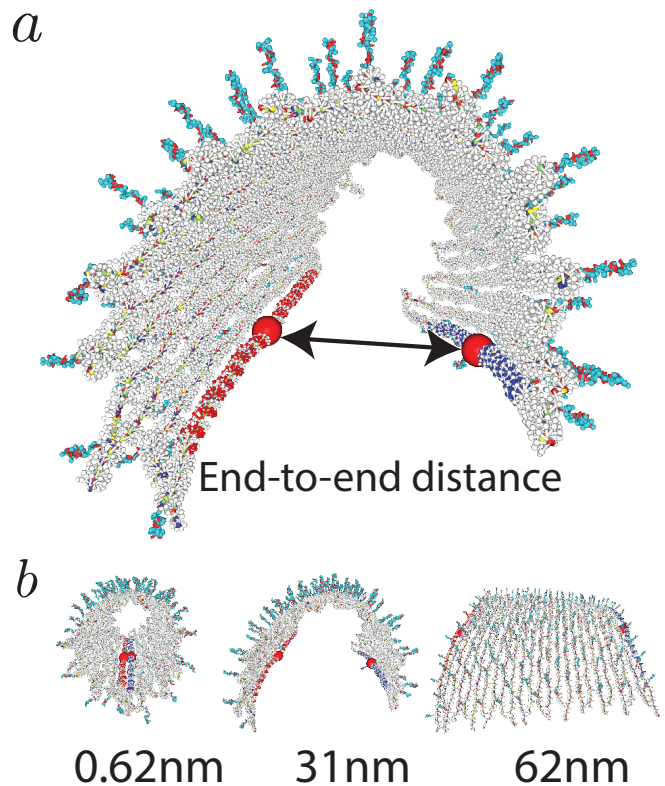


FIG. 2. (*a*) Mean structure of twist-corrected rectangular origami with 169 overhang extensions comprised of twenty nucleotide bases. The arrows indicate the measured end-to-end distance order parameter (R_{ee}) used to model the curvature of the structures. Low R_{ee} values correspond to high curvatures and high R_{ee} ’s to low curvatures. (*b*) Mean structures of umbrella simulation windows equilibrated around 0.62 nm, 31 nm, and 62 nm respectively.

The primary model system we chose to study the structural impact of DNA origami functionalization though extending staple strands was the twist-corrected rectangular DNA origami from Ref. [31] (shown on the left in

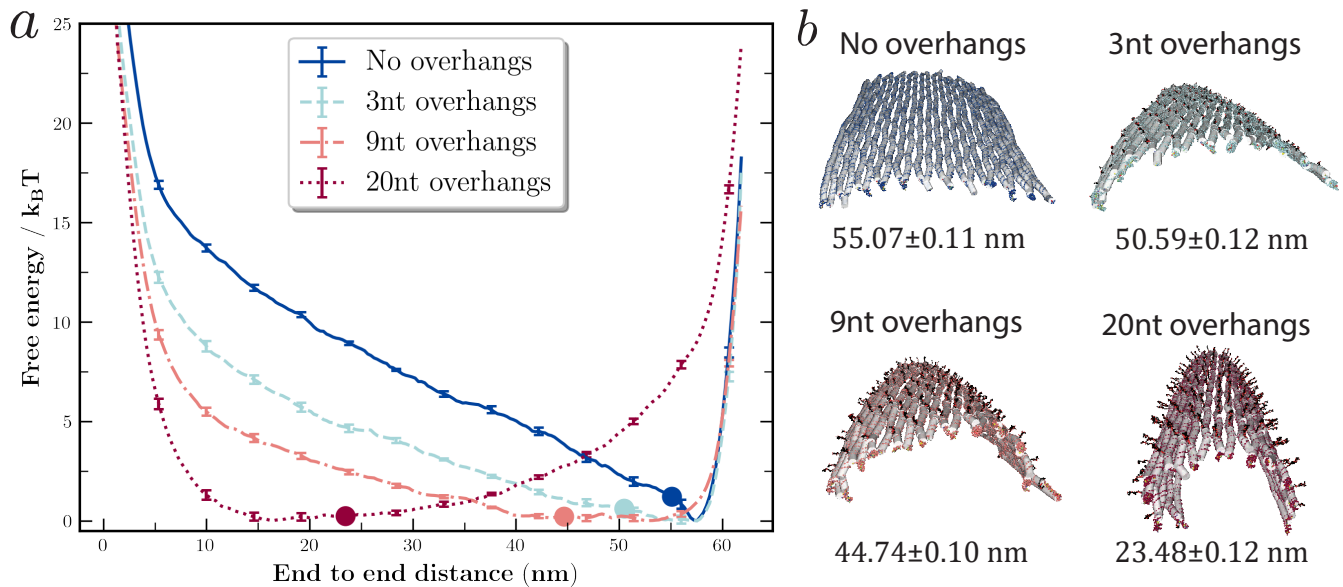


FIG. 3. Effect of overhang length on structural curvature. (a) Free energy profiles as a function of the end-to-end distance of the twist-corrected rectangular tile origami. The dots indicate the location of the weighted average value. (b) oxView visualization of mean structures and corresponding weighted average values. We compared structures with no overhangs, 3nt, 9nt, and 20nt overhangs. The free energy profiles show that structures with a greater number of nucleotides in the overhangs, effectively longer overhang length, exhibit higher probabilities to be in states with higher magnitudes of curvature.

Fig. 1a). The DNA origami rectangles of this type have been utilized in various applications as a molecular canvas for nanometer scale positioning due to the ~ 5 nm resolution of the site specific addressable DNA overhangs [31]. We extended DNA overhangs from the 5' ends of the origami's staple strands, using a multitude of overhang conditions including single-strands, double-strands (169 overhangs, 85 overhangs), as well as varying their length. To model experimentally realized systems, we initially created structures with nine nucleotide (9nt) and twenty nucleotide (20nt) long overhang extensions. The 9nt overhang structure models the qPaint docking strand system from Ref. [31] and the 20nt structure represents the molecular positioning system created by Gopinath and collaborators in Ref. [32].

Initial unbiased oxDNA simulations indicated the presence of structural curvature upon extension of overhangs, as can be seen in the calculated mean structure (Fig. 2a). We next employed umbrella sampling to quantify the magnitude of curvature in rectangular origami structures with overhangs. Umbrella sampling (US) is an enhanced sampling technique that allows us to efficiently sample all values along our chosen order parameter (OP) by introducing an external harmonic potential that biases the simulation to sample all desired states of the OP that represents different conformations of the structure (see Methods) [23, 33–35]. To model structural curvature, we chose our OP to be the distance between the centers of mass (COM) of the origami's long edges (see Fig. 2), titled as the end-to-end distance (R_{ee}), following the approach from Ref. [34].

The simulations allow us to assign probabilities to

observe particular values of our OP in the conformational ensemble, which we use to quantify the rectangular origami's preference to exhibit different magnitudes of curvature as a function of the end-to-end distance between edges of the origami (R_{ee}), as it represents a one-dimensional description of the curvature. The R_{ee} was sampled from 0.62 nm to 62 nm.

In addition to the 2D origami from Ref. [31], we used oxDNA simulations (with similar OP choice, see Methods) to study the bending of the anti-parallel double layer rectangular origami from the work of Thubagere et al. [29] and the six helix bundle rectangular origami from Dong et al. [36]. We studied their conformations both with and without 20nt long overhangs (see Fig. 7).

To compare the curvature exhibited by different structures, for all the studied designs we plot the free energy as a function of the end-to-end distance (R_{ee}), obtained from the probability $p(R_{ee})$ as $F(R_{ee})/k_B T = -\ln p(R_{ee}) + C$, where we set constant C such that $F(R_{ee})$ is equal to 0 for the most probable value of R_{ee} (i.e. in its minima) [37]. For each studied system, we also highlight in the plot (as a colored dot) the weighted average end-to-end distance $\langle R_{ee} \rangle_p = \sum_{R_{ee}^i} p(R_{ee}^i) R_{ee}^i$, where R_{ee}^i are all the binned values of the end-to-end distance of R_{ee} that were sampled during the simulation.

B. Effects of Overhang Length

To investigate the impact that different lengths of overhang extensions had on inducing the rectangular origami to curve, we simulated structures with varying num-

ber of nucleotides in their single-stranded poly-T overhangs. Free-energy profiles were computed for a rectangular structure with no overhangs, and then for three nucleotides, nine nucleotides, and twenty nucleotide-long overhangs respectively. All considered systems had the same density of overhangs, 169 overhangs in total attached to the 2D origami tile. We observe that the umbrella sampling simulation results show significant curvature in all origami structures with added overhang extensions. With the increasing length of the overhang, the probability of exhibiting a greater magnitude of curvature also increased (Fig. 3).

The rectangular structure with zero overhangs showed a weighted average R_{ee} value of 55.07 ± 0.11 nm, while the 3nt, 9nt, and 20nt overhang structures had weighted average values of 50.59 ± 0.12 nm, 44.74 ± 0.10 nm, and 23.48 ± 0.12 nm respectively (shown as colored dots in Fig. 3). These values quantitatively show a significant difference in the average curvature of the four different structures, where longer overhangs lead to increased curvature.

Further, while the weighted average values are valuable for comparisons of curvature between different structures, the individual flexibility of a structure can be seen from the differences between end-to-end distance free-energy profiles for the respective overhang lengths studied (Fig 3). From the relative flatness of the free-energy profiles, it can be seen that the structures have immense flexibility in exploring conformations outside of the minimum. For example, the 2D origami with 9nt overhangs has a free energy minimum at $R_{ee} = 48$ nm, but is only about 7 times less likely to visit R_{ee} values of 30 nm and 150 times less likely to visit R_{ee} values of 7 nm, and hence it is expected to sample these conformations frequently in the bulk. Thus, to understand both the structure and how flexible DNA origami will behave in solution and how likely certain conformations are, it is vital to obtain more accurate and complete information than static structural properties (e.g. AFM image) can provide us.

C. Entropy as the Driving Force

To study the cause behind the induction of curvature through the addition of overhang extensions, we performed simulations with a modified oxDNA model where non-bonded interactions were turned off between specific groups of nucleotides for the origamis with 9nt and 20nt long single-stranded overhangs. We expect that the excluded volume interactions (two strands cannot occupy the same space at the same time) are the primary driving force behind the observed curvature. The single-stranded overhangs need to avoid overlapping with each other. The likelihood that two of the neighboring overhangs will clash with each other is lower if the 2D origami is curved. Furthermore, the amount of volume accessible to an overhang strand (Fig. 1c) will increase (Fig. 1d) if the 2D origami bends more, thus making the bent configuration

more favorable for entropic reasons, as the overhangs will have larger conformational volume accessible.

To study these phenomena, we simulated three different system modifications to decompose the underlying effects of the curvature. In the first modification, we explicitly switched off in the simulations all interactions between all pairs of overhangs, allowing the overhangs to pass through each other. For the second modification, we switched off interactions between the nucleotides in the single-stranded overhang extensions and the nucleotides in the rectangular origami's base, thus allowing the overhangs to freely pass through the origami surface. Finally, in the third modification, we combined both prior approaches and switched off the interactions between the overhangs with the rectangular tile as well as interactions with other overhangs. For each of the modified simulations, we ran umbrella sampling simulations to reconstruct the free-energy profile of the end-to-end distance R_{ee} for the systems with 9nt and 20nt long single-stranded overhangs (Fig. 4).

Analyzing the modified simulations for the 20nt overhangs structure, the free-energy profile for the first modification (interaction of overhangs with other overhangs switched off) moderately shifts the weighted average of the R_{ee} from 23.48 ± 0.12 nm to 37.66 ± 0.17 nm. The second modification (overhangs interaction with DNA origami surface switched off) heavily shifted the average R_{ee} values to 54.04 ± 0.13 nm, corresponding to structure with greatly reduced curvature. The third condition (interaction with other overhangs and DNA origami surface switched off) has a weighted average R_{ee} of 54.78 ± 0.14 , nearly identical to the flat DNA origami with no overhangs.

The change in the R_{ee} value for the 9nt long overhangs shows a different trend for the first modification (no interactions between overhangs), as the free-energy profile remains nearly identical as to the case where no modification is introduced, implying that for these short overhangs, the effects of overhangs interacting through excluded volume are negligible. The second modification (switching off interactions between overhangs and DNA origami surface) shows an increase in the average R_{ee} value from 44.74 ± 0.10 nm to 53.62 ± 0.10 nm, corresponding to decrease in curvature. Thus, for shorter overhangs, the entropic origin of curvature appears to be only due to the increased conformational space of individual overhangs, rather than due to the clashes with other overhangs.

Overall, these results show that the interactions between the overhang extension with the rectangular tile structure are the main contributing factor in causing the rectangular origami to curve. By adopting a curved surface, the number of conformational states that the overhangs extensions are able to explore increases, and consequently the curved structure is entropically favored (Fig. 1C,D).

In addition to the curvature caused by the interaction between the overhangs and the rectangular tile, the in-

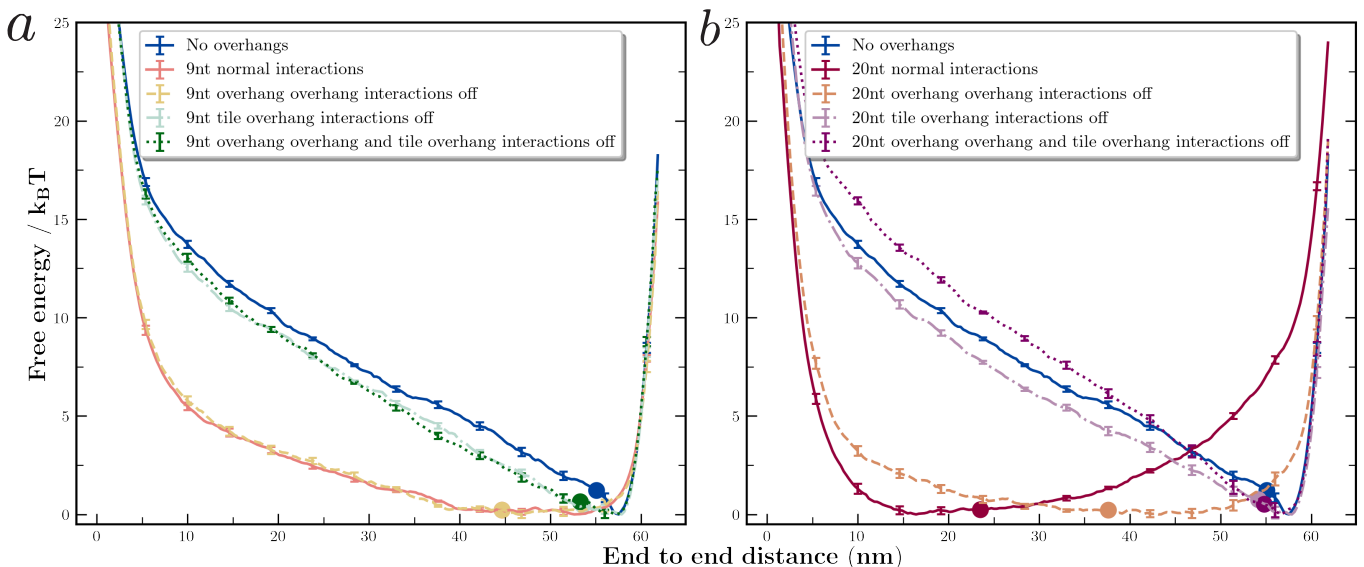


FIG. 4. Entropy as the Driving Force. Non-bonded interaction potentials of the overhang extensions for the (a) 9nt and (b) 20nt systems were modified to decompose the source of curvature. When the interactions of the overhangs with the rectangular tile are switched off the curvature of both systems closely mirrors the zero overhang curvature, indicating this interaction to be the main source of curvature. When the overhangs interactions with other overhangs are turned off the 20nt system has a moderate change in curvature while the 9nt system does not change, leading to the conclusion this condition is impactful only for long overhangs.

interactions between the overhangs themselves also influence the curvature, but the result is only observed for longer extensions. Even though the typical distance between 9nt long overhangs are such that they are able (in a rare case) to potentially overlap, it does not meaningfully reduce the state-space accessible to the overhangs and hence does not affect the curvature of the DNA origami tile.

D. Effects of Overhang Duplexes and Density

To analyze the effect of overhang extensions in complex with their complementary strands as well as different densities of overhangs, we designed and simulated origami structures with 169 duplex overhangs ("dense" system), and "half-dense" structures with 85 single-stranded overhangs and finally structures with 85 duplex DNA overhangs ("half-dense" double-stranded). The double-stranded DNA overhang structures were designed to model a rectangular tile system in complex with complementary functionalized DNA strands. The half density structures are a model for a system in which further precision in the locations of the overhang extensions are necessary, leading to a reduced number of rationally placed overhangs.

The free-energy profiles (see Fig. 5) show that the formation of DNA duplex overhangs increases the curvature of both the 20nt and 9nt duplex overhang structures relative to their single stranded counterparts. While the free-energy minima of the 20nt duplex overhang structure does not change compared to the 20nt single-stranded

overhang structure, an effective overall decrease in curvature can be seen from the shift in the weighted average value. The weighted average R_{ee} for the 20nt duplex overhang structure was 18.03 ± 0.17 nm, as compared to 23.48 ± 0.12 nm for the 20nt single-stranded overhang structure. Similarly for the 9nt long overhangs, the weighted average decreased to 33.20 ± 0.14 nm for the duplex overhangs from 44.74 ± 0.10 nm for the single-stranded overhangs, in addition to a shift in the free-energy minima from 35 nm to 48 nm. Our simulations show that once our rectangular DNA origami structure with dense overhangs is functionalized by binding the overhangs by a complementary strand (and thus creating duplex overhang), the flexible structure will experience further curvature.

We further observed that when the density of the overhangs was approximately cut in half from 169 to 85, the curvature of the structure decreases (Fig. 5), consistent with the fact that the entropic advantage of bending the origami will be lower for smaller number of the overhangs. We next compared the double-stranded overhangs and single-stranded overhangs for the half-density systems with 85 overhangs. Just as we observed for the dense system with 20nt nucleotide long overhangs, the 20nt duplex overhangs structure had increased curvature (average $R_{ee} 45.23 \pm 0.24$) compared to the single-stranded ones (average $R_{ee} 48.87 \pm 0.18$). However, we observe that 9nt duplex overhangs weighted mean end-to-end distance is slightly higher (less curved structure) than for the 9nt single-stranded duplex, which is the opposite effect from what we observed for the dense system with 169 overhangs.

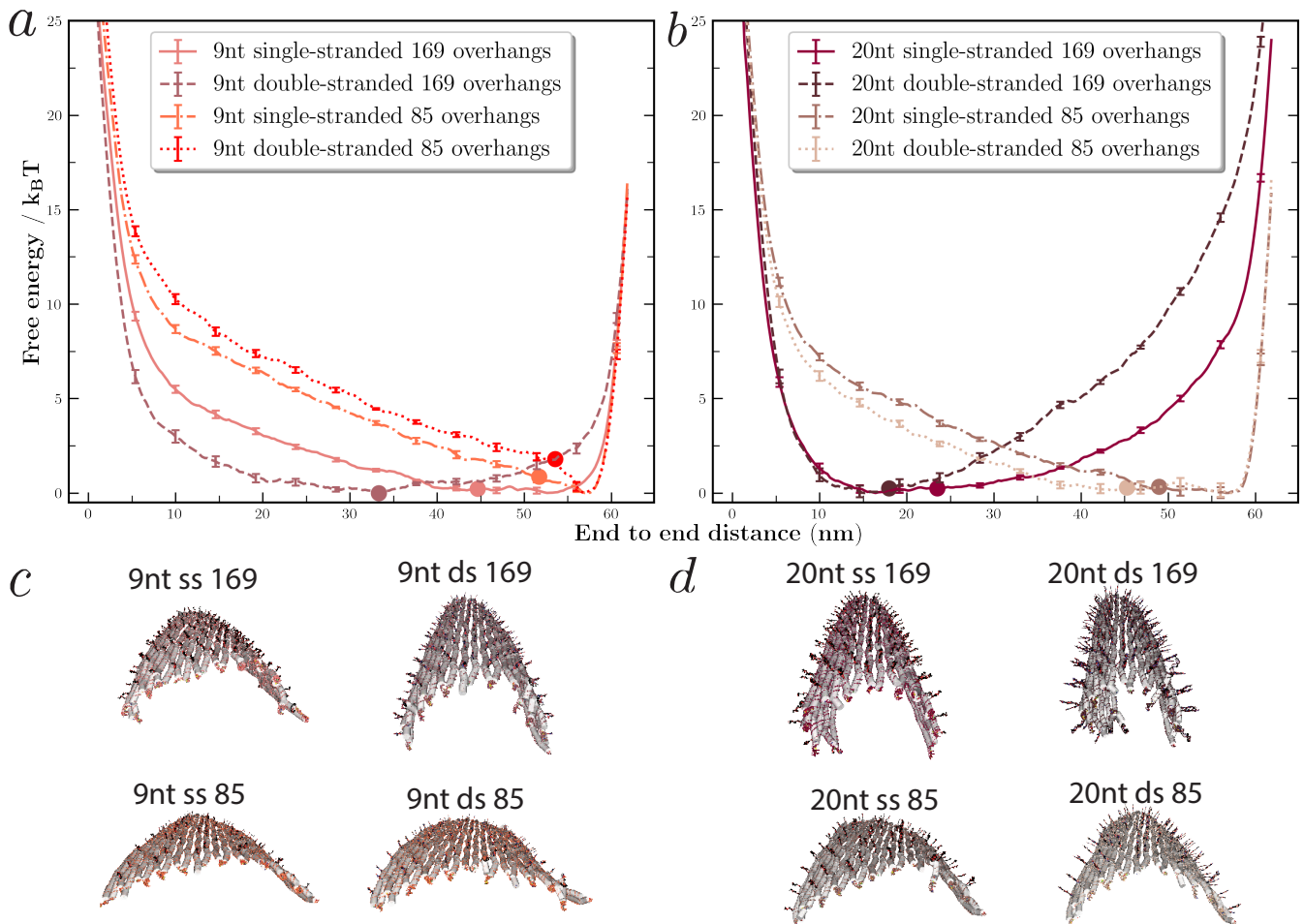


FIG. 5. Effect of different overhang conditions. Free energy profile of (a) 9nt and (b) 20nt modified overhang systems. When the complementary strand of the overhang extension is added to create double-stranded overhangs, the curvature of both the 9nt and 20nt structures increases. Inversely, if the number of single-stranded extensions is reduced to 85 overhangs, the curvature of the structures decrease. Mean structures of (c) 9nt and (d) 20nt overhang conditions illustrate these differences.

The duplex overhangs behave more like wider stiff rods, whereas single-stranded DNA overhangs behave as freely-jointed chains with excluded volume. Thus, we expect the entropic penalty due to the overhangs clashing with other overhangs to increase with double-stranded overhangs compared to single-stranded, an effect which is more pronounced for the longer (20nt) overhangs. However, the fact that the structure with 9nt single-stranded overhangs is slightly more curved than DNA origami with 9nt duplex overhangs, is indicative that the duplex overhangs are clashing less with the DNA origami surface than the single-stranded ones.

Finally, the sequence effects of the single-stranded regions was investigated by using the sequence-dependent version of the oxDNA model [18], which has parameterized stronger Adenine-Adenine stacking compared to Thymine-Thymine stacking. The simulations (Supp. Materials Fig. S2) showed that there was no effective difference in the curvature of the structures when the nucleotide sequence was Thymine or Adenine and hence that the greater tendency for adenine's to stack com-

pared to thymine does not affect the origami's structural curvature.

E. Effects of Temperature and Salt Concentration

In all cases considered above, we fixed temperature to 20°C and salt concentration in the oxDNA model to 1M. To characterize how the curvature of the rectangular tile origami might respond to different temperatures and salt concentrations, we computed free-energy profiles of end-to-end distance at four different temperatures and salt concentrations for the 20nt long single-stranded overhang and no-overhang DNA origami structures. Simulations were run at 10°C, 20°C, 30°C, and 40°C as well as at salt concentrations of 0.2 M, 0.6 M, 0.8 M, and 1 M (shown in Fig. 6).

The free-energy profiles of end-to-end distance (and hence the curvature of the DNA origami) change only slightly between different temperatures, corroborating the entropic origin of the curvature.

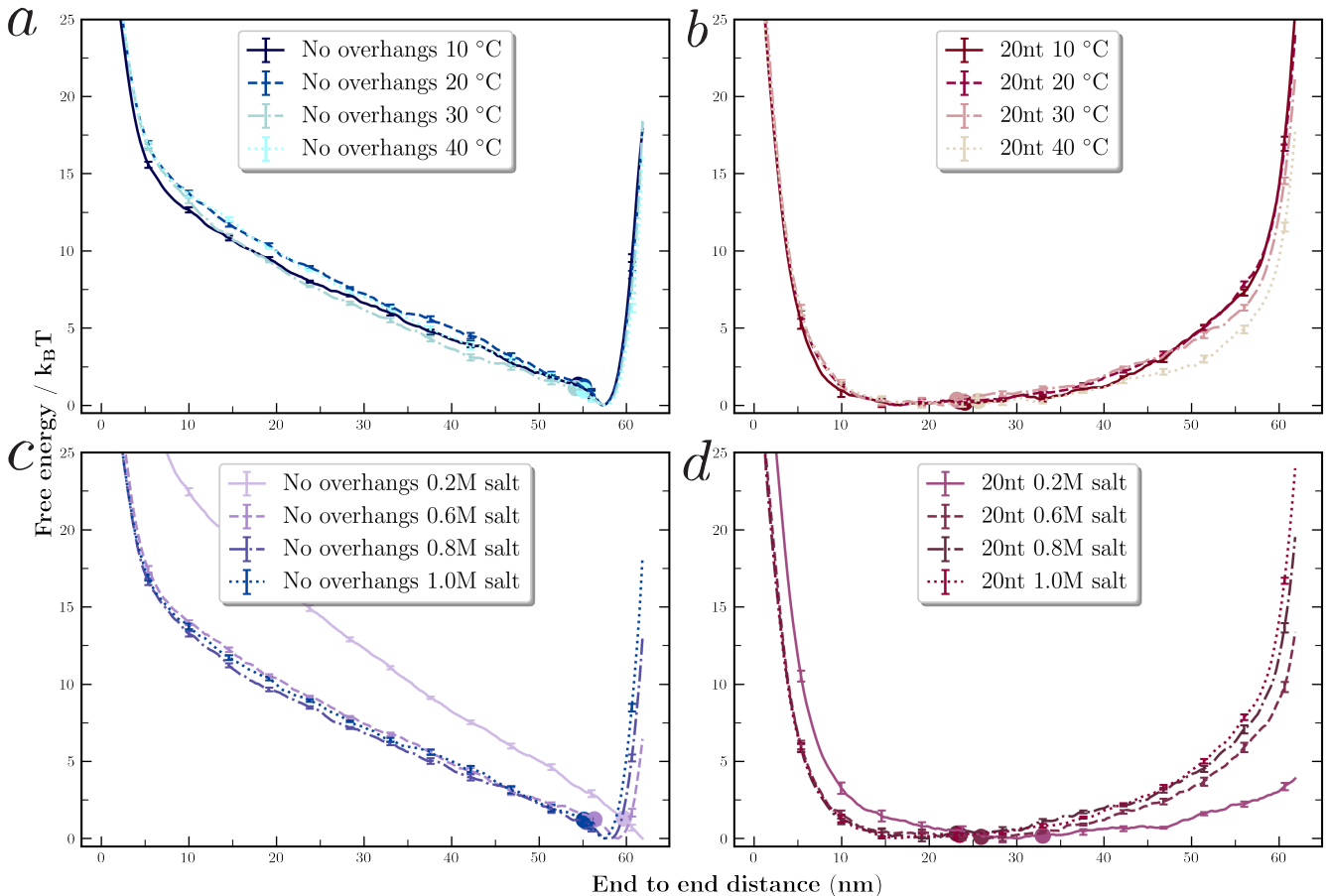


FIG. 6. Effect of different temperatures and salt concentrations. Free energy profiles of (a, c) no overhangs and (b, d) 20nt overhangs at various temperatures and salt concentrations. For both no overhang and 20nt structures, when the temperature is increased the curvature is negligibly effected. When the salt concentration is decreased, the curvature of the structure decreases due to the increase in electrostatic repulsion between charged backbone sites in the rectangular tile.

When the salt concentration is varied, we see that as the salt concentration decreases, the curvature of the structure also decreases. Our oxDNA model implements salt effects using Debye-Hückel potential [18], where the backbone sites of the nucleotides in the model interact with repulsive interaction with an effective charge. With decreasing salt concentration, the effective excluded volume occupied by the overhangs increases, and while the curvature does not change drastically from 1 to 0.6 M salt, we observe moderately less curvature for 0.2 M salt. The large magnitude change in curvature for 0.2 M salt as compared to other salt concentrations can be attributed to the exponential increase in the Debye length as the salt concentration approaches 0. The increased electrostatic repulsion between the nucleotide backbones in the origami helices effectively flattens the structure, as can be seen for system with no overhangs (Fig. 6). For the 20nt overhang lengths, while they have larger excluded volume at lower salts, the flattening of the origami at low salt concentrations still leads to larger average R_{ee} (smaller curvature) at lower salt concentrations.

F. Anti-Parallel Double Layer and Six Helix Bundle Rectangles

To compare the effects overhang extensions have on 3D rectangular structures as opposed to the 2D structure, we simulated two rectangular origami planes with 3D architectures. One of the structure is made of two anti-parallel 2D rectangles (Fig. 7b), while the other is a rectangle made of six helix bundles (Fig. 7c) [29, 36]. We extended twenty nucleotide overhangs from the staple strands of both systems.

The free-energy profiles of both of the 3D rectangular structures show a immense increase in structural rigidity. The steepness of the free-energy profiles around the free-energy minimum as compared to the single layer 2D rectangular origami indicates that the end-to-end distance between edges of the structures are nearly constant, with huge penalty for bending. The anti-parallel structure (Fig. 7b) has a free-energy minimum of end-to-end distance at 50.45 nm and weighted average of 50.49 ± 0.02 nm, and similarly the six helix bundle (Fig. 7c) has a minimum of 49.95 nm and a weighted average of 50.04 ± 0.03 nm. In comparison, the single layer DNA origami with

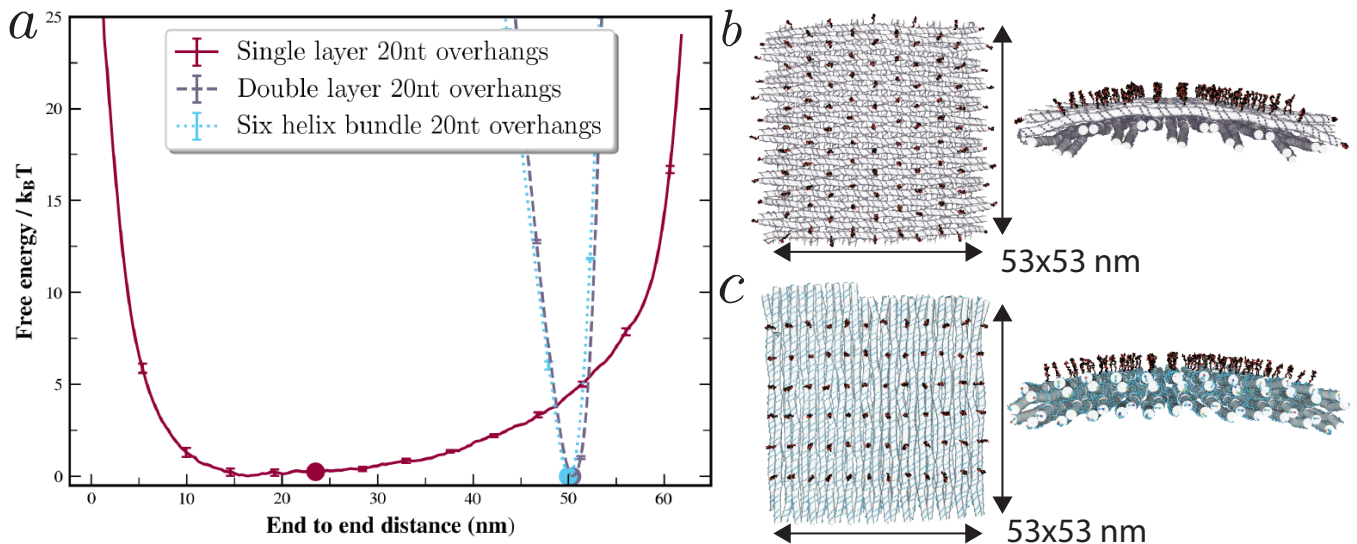


FIG. 7. (a) Free-energy profiles of 3D rectangular origami structures. (b) The double layer anti-parallel 20nt overhangs and (c) six helix bundle 20nt overhangs structures show a remarkable increase in rigidity compared to the 2D rectangular structure. The anti-parallel and six helix bundle free energy profiles show a much steeper rise in free energy upon perturbations from the free energy minimum indicating low flexibility, with weighted averages at 50.49 ± 0.02 nm and 50.04 ± 0.03 nm respectively.

20nt overhangs that we studied in previous sections has an end-to-end distance minimum at 16.42 nm and a weighted average of 23.48 ± 0.12 nm, which is due to an underlying skewed distribution with a higher probability for states beside the minimum. In contrast, the measured values for 3D double-layered structures indicate a rigid body with a large free-energy penalty for perturbations away from the minimum. We note that these 3D designs are preferred choice for application where flexibility of the structure should be minimal and prevent any cross-talk between the molecules attached to the structure surface [29].

III. DISCUSSION AND CONCLUSIONS

In this study we characterized the effect of site addressable functionalizable overhang extensions on the structure of twist-corrected rectangular DNA origami. We showed that upon extension of overhangs from the end of staple strands, there was a significant induced curvature in the structure. Furthermore, we quantified how the average curvature is influenced by different variables including the overhang length, single-stranded versus double-stranded overhangs, density of overhangs, overhang sequence, temperature, and salt concentration. The insights provided by the computed free-energy profiles paint a robust picture of the dynamics of flexible DNA origami in solution. These results conclude that in order to rationally design flexible DNA nanostructures with nanometer scale precision, it is vital to take into account the effect that extensions will have on modifying the resultant structure.

While in the past experimental evidence indicate the existence of this phenomenon [38–40], this study was

the first to rigorously quantify the degree of curvature induced by the functionalization of origami by single-stranded and double-stranded overhangs, with implications for designs with other guest molecules (such as proteins or gold nanoparticles), which we expect to show effects. We showed that as the number of nucleotides in the overhang extensions increases, the average curvature of the rectangular origami increases as well. In addition, we displayed how the curvature of the origami structure increased as a response to the formation of double stranded DNA overhangs.

By sampling the dynamics of an implicitly solvated DNA origami, oxDNA accurately predicts how entropic effects impact structural properties. Utilizing modified interaction potentials, we decomposed the entropic penalty caused by excluded body steric interactions. The increased state space accessible to the overhang extensions upon origami curvature results in a free energy landscape with a high probability of curved states.

Furthermore, when the simulations of DNA origami are utilized to calculate free-energy profiles through umbrella sampling simulations, we are able to obtain a much more robust characterization of not only the mean conformation of our nanostructure, but also obtain information on all possible states, along with the associated probability, of flexible DNA origami.

Finally, we ran oxDNA molecular dynamics simulations of 3D anti-parallel double layer rectangular DNA Origami and a six helix bundle rectangular DNA Origami with 20nt overhang extensions. The simulations showed that there was a significant increase in structural rigidity with negligible deformation of the planar shape of both 3D nanostructures as compared to the 2D rectangular origami. Hence, 3D DNA origami rectangles would be recommended in an application where a planar structure

is required or precise spatial resolution needs to be retained upon overhang functionalization.

Overall, our findings provide an important quantification of the effects of functionalization of the DNA origamis on their conformational ensemble, with implications for functional designs for fields such as photonics, diagnostics and drug delivery. We also note the effect of origami curvature induced by overhangs can be potentially exploited to induce desired curved shape on a DNA origami surfaces. The typical conformation for all the structures that have been simulated are provided in the Supp. Mat. (Fig S3) and summarized in Supp. Mat. Table S1.

We make the computational methods and all the software tools developed here to setup umbrella sampling of conformations of nanostructures with oxDNA model at https://github.com/mlsample/ipy_oxDNA.git, along with tutorials and examples. We also provide an automated setup that allows to run multiple instances of oxDNA molecular dynamics simulations on a single GPU card. With our setup, we were able to run in parallel on 40 oxDNA simulations of a single DNA origami on one 40GB NVIDIA A100 card. Running simulations in parallel on a single card is multiple times faster than running one simulation after other. We observed an increased throughput of 2 times for 5 simulations or 2.6 times for 40 simulations in parallel on a single GPU card. Hence, our setup opens a way for massively parallelized nanostructure characterization even with limited computational resources.

IV. METHODS

To simulate the structural dynamics of the DNA nanostructures, we use the oxDNA coarse-grained model. Specifically, we used oxDNA2 [18] implemented on GPU [25, 26]. The time-step used for all simulations was 0.005 in internal oxDNA units as done by Wong et al. [34]. Simulations were performed at 293.15 K and 1 M salt concentration with averaged stacking and hydrogen bonding unless otherwise specified. An Anderson-like thermostat was used for temperature coupling and the salt concentration is modeled using the Debye-Hückel potential. A diffusion coefficient of 2.5 in simulation units was used, enabling us to sample longer timescales. The starting configurations were prepared by the oxView tool [41, 42], where we extended a specified number of staple strands to the 5' end of the 2D rectangular origami tile.

Umbrella sampling [43, 44] was then used to compute all of the free energy profiles in this study. Adopting the approach from Ref. [34], we introduced a biasing harmonic potential $V_{\text{bias}} = \frac{k}{2}(R_{\text{ee}} - R_0^{w_i})^2$, where R_{ee} is the distance between the centers of mass of the edges of the DNA origami, and $R_0^{w_i}$ is a variable that is selected for a particular simulation window. For each studied system, we simulated multiple independent windows, where a window is a standalone simulation that was run for 20

million simulation steps. For each window w_i , we set a different value of $R_0^{w_i}$, ranging from 0.62 to 62 nm using 100 simulation windows with the increment between each window being 0.62 nm. The maximum order parameter value was 62 nm, was chosen because the average R_{ee} of the rectangular structure when forced to be flat using a repulsion plane external potential was calculated to be about 60 nm, and we aimed to profile the structure slightly beyond flat leading to our choice of 62 nm as the maximum value. The minimum value of 0.62 was picked as a result of our decision to use 100 simulation windows, where 100 windows starting at 62 nm decreased by 0.62 nm over our windows leads to a minimum value of 0.62 nm. We chose 100 simulation windows and the biasing harmonic potential with a spring constant $k = 11.418$ pN/nm to guarantee sufficient overlap between neighboring windows. The R_{ee} was fit to the angle between the center of the rectangle and the ends using polynomial fitting Supp. Mat. (Fig S1).

Once the 100 production windows were run, we used the Weighted histogram analysis method [43–45] (WHAM) to unbias our simulations results and provide free energy values as a function of our order parameter. We chose to use 200 bins for our WHAM analysis. The plotted free energy over $k_B T$ is calculated by dividing the WHAM calculated free energy by the temperature. We used Ref. [45] for Monte Carlo bootstrapping error analysis to create the error bars on the free energy values, which are also divided by the temperature of the system. Using the free-energy values calculated from WHAM, the weighted average of the end-to-end distance is then computed, using the probability of respective end-to-end values. The error of the weighted average was computed using parametric bootstrapping, modeling the free energy profiles as a multivariate Gaussian with means equal to the free energy values and standard deviations equal to the error provided by the WHAM Monte Carlo bootstrapping error analysis.

V. ACKNOWLEDGMENTS

We acknowledge support from the ONR Grant N000142012094 and DURIP ONR grant no. N000142112876. We further acknowledge use of the Extreme Science and Engineering Discovery Environment (XSEDE), which is supported by National Science Foundation grant number TG-BIO210009. We thank Jonathan Doye, Thomas Ouldrige, Paul Rothemund, and Matteo Guareschi for helpful discussions and to Joel Joseph for help with the design of the simulated structures.

Supporting Information

S1. UMBRELLA SAMPLING

A. Background

Umbrella sampling is an enhanced sampling molecular dynamics technique utilized to calculate free energy profiles as a function of a chosen order parameter. A order parameter is chosen for its ability to represent a phenomenon of interest. The umbrella sampling technique uses multiple simulation replicas called windows, where each window samples a different subset of your order parameter. By applying a biasing potential, called the umbrella potential, to each simulation window we are able to explicitly sample the entire range of values along the axis of our order parameter. After all simulation windows have run, we unbias the simulation results using the Weighted Histogram Analysis Method (WHAM)[43–45]. Using multiple simulation replicas to sample different order parameter values relevant to our phenomenon of interest decreases the time required for our free energy profile to converge.

B. Order Parameter

To quantify the curvature of the rectangular structure the order parameter we chose was the distance between the center of mass of the scaffold nucleotides along the long edge of the rectangular structure, called the end to end distance (R_{ee}). We excluded nucleotides at the corners of the rectangular structure from our order parameter as they experience large magnitude random fluctuations and transient hydrogen bond fraying.

The R_{ee} was chosen for a few reasons. First, the relationship between the distance of the two ends and the angle theta (shown in Fig S1) provides an metric to quantify the relative curvature of the rectangular origami. Additionally, as R_{ee} is a 1D parameter, we get faster convergence of our free-energy landscapes as sampling all possible values of a single degree of freedom can be done quickly. Finally, as our chosen umbrella potential was a COM harmonic biasing potential, choosing an OP based on the distance between two centers of masses enables us to directly bias our structures to sample our OP.

The value of R_{ee} was sampled from 0.62 nm to 62 nm. A hundred windows were used where each window sampled OP values biased to fluctuate around specific R_{ee} values. Equally spaced increments of 0.62 nm along the 1D axis of the OP were used. The extrema values of R_{ee} was chosen by performing pulling simulations on the 0 overhang structure using an external attraction plane potential.

The attraction plane potential was applied to all nucleotides in the system, pulling them towards a plane on the x-y axis with a stiffness of 0.1 pN/nm per nucleotide.

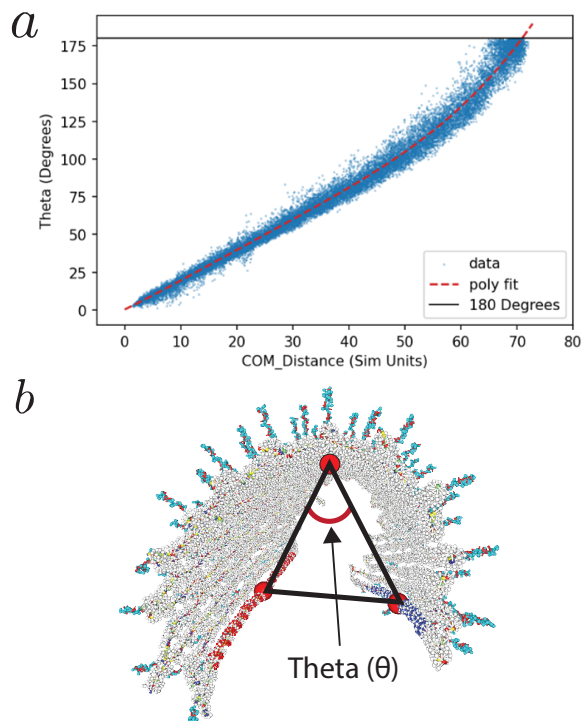


FIG. S1. (a) The angle theta as a function of the end-to-end distance was fit using polynomial regression. Theta was calculated by measuring the three distances shown in b) and using the law of cosines relationship to get theta. The fit shows that as the value of R_{ee} increases the angle theta also increases. As a theta value of 180° indicates a flat structure, as R_{ee} increases the curvature decreases.

oxView was then used to identify the nucleotide IDs along each of the rectangles long edges and oxDNA-analysis-tools was used to calculate the mean distance between the COM of the two edges. An extra 2 nm was added to the mean distance and used as the max R_{ee} distance (62 nm) to sample states beyond the most stable flat structure.

C. Running Umbrella Sampling

We have provided an interactive Jupyter notebook to automate the majority of the tasks required to run umbrella sampling which can be found here: https://github.com/mlsample/ipy_oxDNA As a prerequisite, oxDNA python environment (oxpy) must be installed. It can be obtained though compiling oxDNA with python support (see <https://lorenzo-rovigatti.github.io/oxDNA/install.html>). The parameters used to run the umbrella simulations can be found the tutorial notebook.

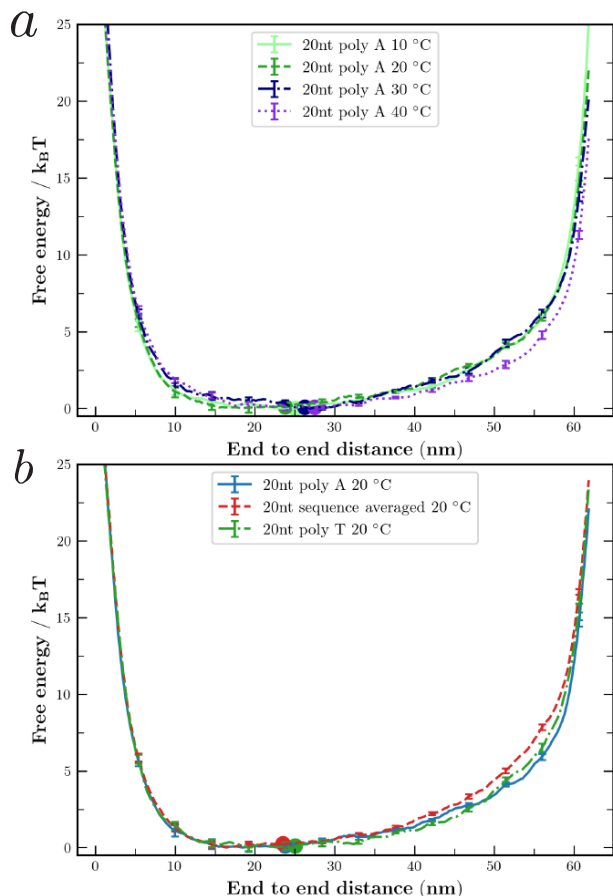


FIG. S2. Effect of overhang nucleotide sequence. The difference between the 20nt poly A and poly T simulations show no significant difference. When the temperature is varied for the poly A structure no large difference is seen for the weighted average.

D. Umbrella Equilibration and Convergence Analysis

To ensure proper equilibration of starting conformations was performed, we trimmed off the first 1 million, 2 million, and 3 million production steps of each simulation window. The trimmed profiles look identical to the profile with all the data indicating that the starting conformation of the umbrella sampling simulations were equilibrated properly. To check convergence we separated the first and last 10 million steps, as well as plotting free energy profiles of data points obtained from 10, 12, 14, 16, and 18 million steps. As the free energy profiles of both the first and last 10 million steps are nearly identical, it can be said that the umbrella sampling simulations have converged. Similarly, as we increased the number of data points the free energy profile negligibly changed as the umbrella windows were run longer.

System	End-to-End Distance	Standard Error of the Mean
0 Hangs 0.2 M Salt	59.77	0.10
0 Hangs 0.6 M Salt	56.33	0.13
0 Hangs 0.8 M Salt	55.37	0.12
0 Hangs 10 °C	54.50	0.13
0 Hangs 20 °C	55.07	0.11
0 Hangs 30 °C	54.07	0.14
0 Hangs 40 °C	55.04	0.13
1nt 20 °C	53.03	0.09
3nt 20 °C	50.59	0.12
9nt 10 °C	42.56	0.14
9nt 20 °C	44.74	0.10
9nt 40 °C	45.71	0.13
9nt Half Density	51.75	0.16
9nt Duplex 10 °C	35.30	0.14
9nt Duplex 20 °C	33.20	0.14
9nt Duplex 40 °C	39.75	0.16
9nt Duplex Half Density	53.70	0.15
9nt Overhang Clashing Off	44.60	0.16
9nt Tile Clashing Off	53.62	0.10
9nt Tile and Overhang Clashing Off	53.36	0.11
9nt Poly T 10 °C	43.98	0.12
9nt Poly T 40 °C	48.52	0.11
20nt 0.2 M Salt	32.88	0.18
20nt 0.6 M Salt	25.81	0.14
20nt 0.8 M Salt	23.14	0.15
20nt 10 °C	24.08	0.21
20nt 20 °C	23.48	0.12
20nt 30 °C	23.03	0.18
20nt 40 °C	25.76	0.14
20nt Half Density	48.87	0.18
20nt Duplex	18.04	0.17
20nt Duplex Half Density	45.23	0.24
20nt Overhang Clashing Off 10 °C	36.15	0.17
20nt Overhang Clashing Off 20 °C	37.66	0.17
20nt Overhang Clashing Off 40 °C	41.48	0.17
20nt Tile Clashing Off 10 °C	53.08	0.13
20nt Tile Clashing Off 20 °C	54.05	0.13
20nt Tile Clashing Off 40 °C	55.26	0.15
20nt Tile and Overhang Clashing Off	54.78	0.14
20nt Duplex 10 °C	16.69	0.16
20nt Duplex 40 °C	19.24	0.16
20nt Poly T 10 °C	23.65	0.22
20nt Poly T 20 °C	25.16	0.16
20nt Poly T 30 °C	23.32	0.18
20nt Poly T 40 °C	26.84	0.15
20nt Poly A 10 °C	25.10	0.14
20nt Poly A 20 °C	23.94	0.19
20nt Poly A 30 °C	26.33	0.14
20nt Poly A 40 °C	27.45	0.12
20nt Double-Layer Anti-parallel 20	50.49	0.02
20nt Six Helix Bundle 20	50.04	0.03

TABLE S1. Weighted average end-to-end distance of all simulated umbrella Conditions

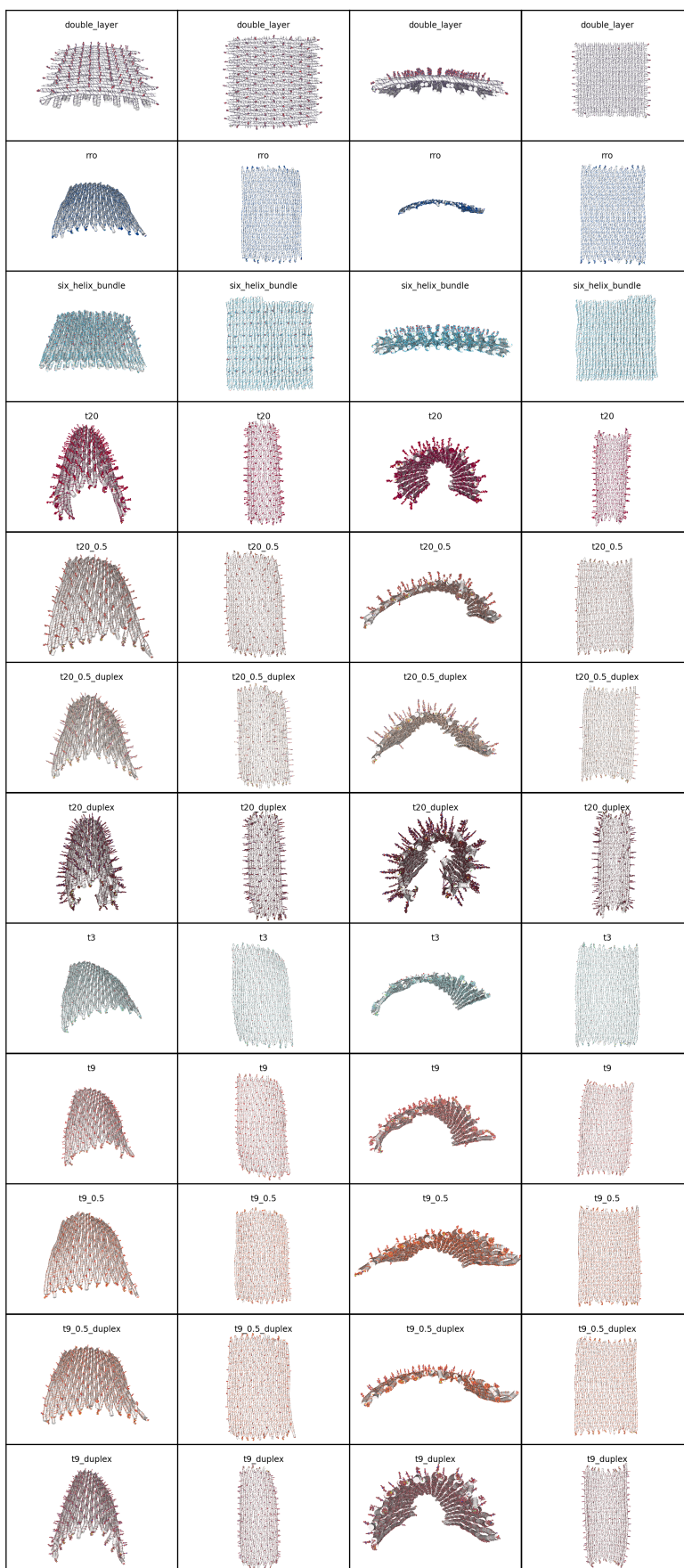


FIG. S3. Means of simulated structures

-
- [1] N. C. Seeman. An overview of structural DNA nanotechnology. *Molecular biotechnology*, 37(3):246, 2007.
 - [2] F. Hong, D. Ma, K. Wu, L. A. Mina, R. C. Luiten, Y. Liu, H. Yan, and A. A. Green. Precise and programmable detection of mutations using ultraspecific riboregulators. *Cell*, 180(5):1018–1032, 2020.
 - [3] P. Guo. The emerging field of RNA nanotechnology. *Nature nanotechnology*, 5(12):833, 2010.
 - [4] A. V. Pinheiro, D. Han, W. M. Shih, and H. Yan. Challenges and opportunities for structural DNA nanotechnology. *Nature nanotechnology*, 6(12):763–772, 2011.
 - [5] J. Kim and E. Franco. RNA nanotechnology in synthetic biology. *Current opinion in biotechnology*, 63:135–141, 2020.
 - [6] P. W. Rothemund. Folding DNA to create nanoscale shapes and patterns. *Nature*, 440(7082):297, 2006.
 - [7] S. M. Douglas, H. Dietz, T. Liedl, B. Högberg, F. Graf, and W. M. Shih. Self-assembly of DNA into nanoscale three-dimensional shapes. *Nature*, 459(7245):414–418, 2009.
 - [8] S. Dey, C. Fan, K. V. Gothelf, J. Li, C. Lin, L. Liu, N. Liu, M. A. Nijenhuis, B. Saccà, F. C. Simmel, et al. DNA origami. *Nature Reviews Methods Primers*, 1(1):1–24, 2021.
 - [9] B. Ding, Z. Deng, H. Yan, S. Cabrini, R. N. Zuckermann, and J. Bokor. Gold nanoparticle self-similar chain structure organized by DNA origami. *Journal of the American Chemical Society*, 132(10):3248–3249, 2010.
 - [10] Q. Pan, C. Nie, Y. Hu, J. Yi, C. Liu, J. Zhang, M. He, M. He, T. Chen, and X. Chu. Aptamer-functionalized DNA origami for targeted codelivery of antisense oligonucleotides and doxorubicin to enhance therapy in drug-resistant cancer cells. *ACS applied materials & interfaces*, 12(1):400–409, 2019.
 - [11] B. Saccà, R. Meyer, M. Erkelenz, K. Kiko, A. Arndt, H. Schroeder, K. S. Rabe, and C. M. Niemeyer. Orthogonal protein decoration of DNA origami. *Angewandte Chemie*, 122(49):9568–9573, 2010.
 - [12] X.-c. Bai, T. G. Martin, S. H. Scheres, and H. Dietz. Cryo-EM structure of a 3D DNA-origami object. *Proceedings of the National Academy of Sciences*, 109(49):20012–20017, 2012.
 - [13] R. Veneziano, S. Ratanalert, K. Zhang, F. Zhang, H. Yan, W. Chiu, and M. Bathe. Designer nanoscale DNA assemblies programmed from the top down. *Science*, 352(6293):1534–1534, 2016.
 - [14] H. Ni, X. Fan, F. Zhou, G. Guo, J. Y. Lee, N. C. Seeman, D.-N. Kim, N. Yao, P. M. Chaikin, and Y. Han. Direct visualization of floppy two-dimensional DNA origami using cryogenic electron microscopy. *Science*, 25(6):104373, 2022.
 - [15] J. Schnitzbauer, M. T. Strauss, T. Schlichthaerle, F. Schueder, and R. Jungmann. Super-resolution microscopy with DNA-PAINT. *Nature protocols*, 12(6):1198, 2017.
 - [16] M. A. Baker, A. J. Tuckwell, J. F. Berengut, J. Bath, F. Benn, A. P. Duff, A. E. Whitten, K. E. Dunn, R. M. Hynson, A. J. Turberfield, et al. Dimensions and global twist of single-layer DNA origami measured by small-angle X-ray scattering. *ACS nano*, 12(6):5791–5799, 2018.
 - [17] T. E. Ouldridge, A. A. Louis, and J. P. Doye. Structural, mechanical, and thermodynamic properties of a coarse-grained DNA model. *The Journal of chemical physics*, 134(8):02B627, 2011.
 - [18] B. E. Snodin, F. Randisi, M. Mosayebi, P. Šulc, J. S. Schreck, F. Romano, T. E. Ouldridge, R. Tsukanov, E. Nir, A. A. Louis, et al. Introducing improved structural properties and salt dependence into a coarse-grained model of DNA. *The Journal of chemical physics*, 142(23):06B613_1, 2015.
 - [19] P. Šulc, F. Romano, T. E. Ouldridge, L. Rovigatti, J. P. K. Doye, and A. A. Louis. Sequence-dependent thermodynamics of a coarse-grained DNA model. *Journal of Chemical Physics*, 137(13):5101, 2012.
 - [20] C. Maffeo and A. Aksimentiev. MrDNA: a multi-resolution model for predicting the structure and dynamics of DNA systems. *Nucleic acids research*, 48(9):5135–5146, 2020.
 - [21] J. G. Lee, K. S. Kim, J. Y. Lee, and D.-N. Kim. Predicting the Free-Form Shape of Structured DNA Assemblies from Their Lattice-Based Design Blueprint. *ACS nano*, 16(3):4289–4297, 2022.
 - [22] D.-N. Kim, F. Kilcherr, H. Dietz, and M. Bathe. Quantitative prediction of 3D solution shape and flexibility of nucleic acid nanostructures. *Nucleic acids research*, 40(7):2862–2868, 2012.
 - [23] B. E. Snodin, J. S. Schreck, F. Romano, A. A. Louis, and J. P. Doye. Coarse-grained modelling of the structural properties of DNA origami. *Nucleic acids research*, 47(3):1585–1597, 2019.
 - [24] X. Wang, S. Li, H. Jun, T. John, K. Zhang, H. Fowler, J. P. Doye, W. Chiu, and M. Bathe. Planar 2D wireframe DNA origami. *Science advances*, 8(20):eabn0039, 2022.
 - [25] L. Rovigatti, P. Šulc, I. Z. Reguly, and F. Romano. A comparison between parallelization approaches in molecular dynamics simulations on GPUs. *Journal of computational chemistry*, 36(1):1–8, 2015.
 - [26] E. Poppleton, M. Matthies, D. Mandal, F. Romano, P. Šulc, and L. Rovigatti. oxDNA: coarse-grained simulations of nucleic acids made simple. *Journal of Open Source Software*, 8(81):4693, 2023.
 - [27] J. P. Doye, T. E. Ouldridge, A. A. Louis, F. Romano, P. Šulc, C. Matek, B. E. Snodin, L. Rovigatti, J. S. Schreck, R. M. Harrison, et al. Coarse-graining DNA for simulations of DNA nanotechnology. *Physical Chemistry Chemical Physics*, 15(47):20395–20414, 2013.
 - [28] A. Sengar, T. E. Ouldridge, O. Henrich, L. Rovigatti, and P. Šulc. A primer on the oxDNA model of DNA: when to use it, how to simulate it and how to interpret the results. *Frontiers in Molecular Biosciences*, 8:693710, 2021.
 - [29] A. J. Thubagere, W. Li, R. F. Johnson, Z. Chen, S. Doroudi, Y. L. Lee, G. Izatt, S. Wittman, N. Srinivas, D. Woods, et al. A cargo-sorting DNA robot. *Science*, 357(6356):eaan6558, 2017.
 - [30] J. Chao, J. Wang, F. Wang, X. Ouyang, E. Kopperger, H. Liu, Q. Li, J. Shi, L. Wang, J. Hu, et al. Solving mazes with single-molecule DNA navigators. *Nature Materials*, 18(3):273–279, 2019.

- [31] R. Jungmann, M. S. Avendaño, M. Dai, J. B. Woehrstein, S. S. Agasti, Z. Feiger, A. Rodal, and P. Yin. Quantitative super-resolution imaging with qPAINT. *Nature methods*, 13(5):439–442, 2016.
- [32] A. Gopinath, C. Thachuk, A. Mitskovets, H. A. Atwater, D. Kirkpatrick, and P. W. Rothemund. Absolute and arbitrary orientation of single-molecule shapes. *Science*, 371(6531):eabd6179, 2021.
- [33] J. Kästner. Umbrella sampling. *Wiley Interdisciplinary Reviews: Computational Molecular Science*, 1(6):932–942, 2011.
- [34] C. K. Wong, C. Tang, J. S. Schreck, and J. P. Doye. Characterizing the free-energy landscapes of DNA origamis. *Nanoscale*, 14(7):2638–2648, 2022.
- [35] C. K. Wong and J. P. Doye. The free-energy landscape of a mechanically bistable DNA origami. *Applied Sciences*, 12(12):5875, 2022.
- [36] R. Dong, T. Aksel, W. Chan, R. N. Germain, R. D. Vale, and S. M. Douglas. DNA origami patterning of synthetic T cell receptors reveals spatial control of the sensitivity and kinetics of signal activation. *Proceedings of the National Academy of Sciences*, 118(40):e2109057118, 2021.
- [37] J. P. Doye, A. A. Louis, J. S. Schreck, F. Romano, R. M. Harrison, M. Mosayebi, M. C. Engel, and T. E. Ouldridge. Free energy landscapes of DNA and its assemblies: perspectives from coarse-grained modelling. In *Frontiers of Nanoscience*, volume 21, pages 195–210. Elsevier, 2022.
- [38] Y. Zhang, Z.-b. Qu, C. Jiang, Y. Liu, R. Pradeep Narayanan, D. Williams, X. Zuo, L. Wang, H. Yan, H. Liu, et al. Prescribing silver chirality with DNA origami. *Journal of the American Chemical Society*, 143(23):8639–8646, 2021.
- [39] A. M. Mohammed and R. Schulman. Directing self-assembly of DNA nanotubes using programmable seeds. *Nano letters*, 13(9):4006–4013, 2013.
- [40] A. Cecconello, J. S. Kahn, C.-H. Lu, L. Khosravi Khorashad, A. O. Govorov, and I. Willner. DNA scaffolds for the dictated assembly of left-/right-handed plasmonic Au NP helices with programmed chiro-optical properties. *Journal of the American Chemical Society*, 138(31):9895–9901, 2016.
- [41] E. Poppleton, J. Bohlin, M. Matthies, S. Sharma, F. Zhang, and P. Šulc. Design, optimization and analysis of large DNA and RNA nanostructures through interactive visualization, editing and molecular simulation. *Nucleic acids research*, 48(12):e72–e72, 2020.
- [42] J. Bohlin, M. Matthies, E. Poppleton, J. Procyk, A. Mallya, H. Yan, and P. Šulc. Design and simulation of DNA, RNA and hybrid protein–nucleic acid nanostructures with oxView. *Nature Protocols*, pages 1–27, 2022.
- [43] G. M. Torrie and J. P. Valleau. Monte Carlo free energy estimates using non-Boltzmann sampling: Application to the sub-critical Lennard-Jones fluid. *Chemical Physics Letters*, 28(4):578–581, 1974.
- [44] G. M. Torrie and J. P. Valleau. Nonphysical sampling distributions in Monte Carlo free-energy estimation: Umbrella sampling. *Journal of Computational Physics*, 23(2):187–199, 1977.
- [45] Grossfield, Alan. "WHAM: the weighted histogram analysis method", Version 2.0.10. http://membrane.urmc.rochester.edu/wordpress/?page_id=126.